



HAL
open science

Water vapor abundance near the surface of Venus from Venus Express/VIRTIS observations

Bruno Bézard, Constantine C. C. Tsang, Robert W. Carlson, Giuseppe Piccioni, Emmanuel Marcq, Pierre Drossart

► **To cite this version:**

Bruno Bézard, Constantine C. C. Tsang, Robert W. Carlson, Giuseppe Piccioni, Emmanuel Marcq, et al.. Water vapor abundance near the surface of Venus from Venus Express/VIRTIS observations. Journal of Geophysical Research. Planets, 2009, 114, 10.1029/2008JE003251 . hal-03785973

HAL Id: hal-03785973

<https://hal.science/hal-03785973>

Submitted on 24 Sep 2022

HAL is a multi-disciplinary open access archive for the deposit and dissemination of scientific research documents, whether they are published or not. The documents may come from teaching and research institutions in France or abroad, or from public or private research centers.

L'archive ouverte pluridisciplinaire **HAL**, est destinée au dépôt et à la diffusion de documents scientifiques de niveau recherche, publiés ou non, émanant des établissements d'enseignement et de recherche français ou étrangers, des laboratoires publics ou privés.

Copyright

Water vapor abundance near the surface of Venus from Venus Express/VIRTIS observations

Bruno Bézard,¹ Constantine C. C. Tsang,² Robert W. Carlson,³ Giuseppe Piccioni,⁴ Emmanuel Marcq,¹ and Pierre Drossart¹

Received 13 August 2008; revised 16 December 2008; accepted 13 March 2009; published 1 May 2009.

[1] Nightside observations of the 1.18- μm atmospheric window by the Visible and Infrared Thermal Imaging Spectrometer (VIRTIS) aboard the Venus Express spacecraft were analyzed to measure and map the water vapor abundance in the lower atmosphere. Thermal emission in this window originates partly from the surface and partly from the first scale height (0–15 km) of the atmosphere. Constraints on the CO₂ continuum absorption, which is the dominant source of gaseous opacity in the window, were obtained from the variation of the 1.185- μm intensity with surface elevation. An absorption coefficient of $1 \pm 0.4 \times 10^{-9} \text{ cm}^{-1} \text{ amagat}^{-2}$ best fits the observed variation. We retrieved a water vapor mole fraction of 44 ± 9 ppm from various selections of VIRTIS spectra in the southern hemisphere, in agreement with previous analyses of the nightside emission. This value is somewhat larger than that previously determined at higher altitudes from the 2.3- and 1.74- μm nightside windows, but the error bars still allow a constant with height H₂O mole fraction from the surface up to 40 km. Using the intensity ratio in the two wings of the 1.18- μm window as a proxy, we searched for horizontal variations of the H₂O abundance in various VIRTIS observational sequences. We derived stringent upper limits for any possible latitudinal variations on the night side: $\pm 1.5\%$ in the range 60°S–25°N and $\pm 3\%$ for the broader range 80°S–25°N. The lack of detectable latitudinal variations is consistent with a constant with height water profile in the lower atmosphere and probably precludes any strong concentration gradient near the surface.

Citation: Bézard, B., C. C. C. Tsang, R. W. Carlson, G. Piccioni, E. Marcq, and P. Drossart (2009), Water vapor abundance near the surface of Venus from Venus Express/VIRTIS observations, *J. Geophys. Res.*, 114, E00B39, doi:10.1029/2008JE003251.

1. Introduction

[2] The near-infrared windows centered at 1.01, 1.10 and 1.18 microns provide a means of probing the lower atmosphere and surface of Venus. In these windows, thermal emission from the surface and the lowest scale height (0–15 km) of the atmosphere can leak through the thick sulfuric acid clouds and be detected on the night side of the planet [Taylor *et al.*, 1997]. The 1.10- and 1.18- μm windows are limited on one side by the $\nu_1 + \nu_2 + \nu_3$ H₂O band centered at 1.13 μm and on the other side by CO₂ bands (respectively the $2\nu_1 + 3\nu_3$ band at 1.05 μm and the $\nu_1 + 3\nu_3$ band at 1.21 μm). Imaging and spectroscopic observations of these windows can thus provide information on the water vapor abundance near the surface and its variations.

[3] Bézard and de Bergh [2007] recently reviewed the determinations of the water vapor abundance in Venus' deep

atmosphere. In the 1990s, various ground-based observations of Venus' night side established that a H₂O mole fraction around 30 ± 10 ppm can reproduce the 1.18- μm window's spectrum [Crisp *et al.*, 1991; Pollack *et al.*, 1993; de Bergh *et al.*, 1995]. From spectroimaging data covering a broad range in surface altitude, Meadows and Crisp [1996] derived a slightly larger H₂O mole fraction, 45 ± 10 ppm. They also argued that the temperature lapse rate in the lowest 6 km is shallower than that measured in situ [e.g., Seiff, 1983] and used in earlier analyses of nightside observations. Reanalyzing Venera 11, 13 and 14 optical spectra, Ignatiev *et al.* [1997] concluded that the H₂O mixing ratio lies between 20 and 40 ppm in the altitude range 5–60 km. Below 5 km, the quality of the Venera data is worse but they seem to indicate an increase of the H₂O mixing ratio up to 50–70 ppm at the surface. All these results show that significant uncertainties remain on the water abundance close to the surface. In particular, analysis of near-infrared windows is hampered by our poor knowledge of the CO₂ "continuum" opacity at high pressures, high temperatures, and long path lengths, arising from collision-induced bands and extreme far wings of allowed CO₂ bands.

[4] Drossart *et al.* [1993] searched for horizontal variations of the H₂O abundance using Galileo/NIMS data

¹LESIA, Observatoire de Paris, UPMC, Université Paris-Diderot, CNRS, Meudon, France.

²Atmospheric, Oceanic and Planetary Physics, Department of Physics, University of Oxford, Oxford, UK.

³Jet Propulsion Laboratory, Pasadena, California, USA.

⁴INAF, IASF, Rome, Italy.

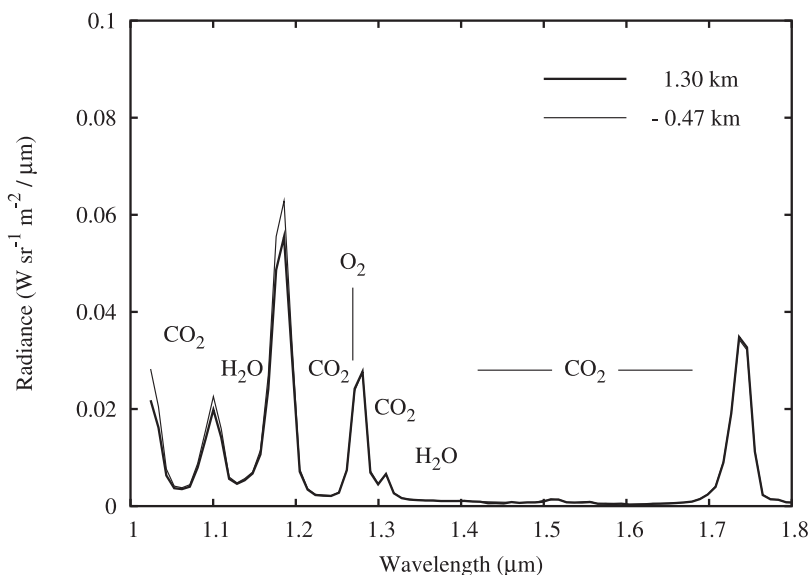


Figure 1. Two averages of 135 Venus' nightside spectra recorded during session 390–13 over Alpha Regio with a mean altitude of 1.30 km (thick line) and about 5° to the east at a mean altitude of -0.47 km (thin line). Emission angle is 45° for both selections. Spectra have been shifted by 7 nm to correct for a slight wavelength calibration error. The location of the main CO_2 and H_2O bands that limit the near-infrared windows is shown along with the position of the O_2 airglow emission.

recorded over a strip on the night side extending from 60°S to 40°N . Analyzing the $1.18\text{-}\mu\text{m}$ window, they concluded that the water abundance in the $0\text{--}15$ km range did not vary by more than 20% over the limited area covered. No other searches for horizontal or temporal variations of water vapor near the surface have been published.

[5] The Venus Express spacecraft, orbiting Venus since April 2006, is currently monitoring the dynamics and composition of Venus' atmosphere. In particular, the Visible and Infrared Thermal Imaging Spectrometer (VIRTIS) is repeatedly mapping Venus' nightside emission through its infrared imaging channel (M-IR), giving access to the composition of the deep atmosphere over large horizontal and temporal scales. We present here an investigation of the water vapor abundance near the surface of Venus using various VIRTIS-M observational sets. We focused on the $1.18\text{-}\mu\text{m}$ window, which is the most favorable, being ~ 3 times more intense than the $1.10\text{-}\mu\text{m}$ one. In a first step, we derived constraints on the CO_2 so-called continuum opacity by investigating the variation of the $1.18\text{-}\mu\text{m}$ emission as a function of the surface elevation. We then determined the H_2O mixing ratio that best reproduces observed spectra. Finally, we analyzed several VIRTIS-M spectral images to search for possible weak horizontal abundance variations, using intensity ratios in the $1.18\text{-}\mu\text{m}$ window as a proxy.

2. VIRTIS Observations

[6] VIRTIS is a dual spectrometer comprising two sub-instruments with their own telescope: an imaging spectrometer (VIRTIS-M) with visible and infrared channels and a high-resolution spectrometer (VIRTIS-H) limited to the interval $2\text{--}5\ \mu\text{m}$ [Piccioni *et al.*, 2007]. The infrared channel of VIRTIS-M covers the range $1.05\text{--}5.2\ \mu\text{m}$ with a spectral sampling of 9.5 nm. The spatial sampling is

0.25 mrad and the instantaneous field of view (FOV) is 0.25×64 mrad, with 256 pixels along the slit. Scanning in the direction across the slit with 256 step positions at 0.25 mrad per step yields a 256×256 image with a 64×64 mrad FOV.

[7] The VIRTIS-M spectral cubes used in this study are listed in Table 1. We selected observational sequences offering all together a good latitudinal coverage from south pole to low northern latitudes ($10\text{--}20^\circ\text{N}$). They usually correspond to off-pericenter observations (Science case 2) except for sequence 093–01, which corresponds to Science case 3 (global spectroimaging from apocenter). The Venus Express science planning is described by Titov *et al.* [2006]. The integration time varies from 3 to 8 s, ensuring a good signal-to-noise ratio on the night side. The sequences marked in bold incorporate regions of relatively high elevation (Alpha Regio, Imdr Regio, Themis Regio) along with regions of low elevation, and have been used to constrain the CO_2 continuum opacity (see section 4.2). Figure 1 shows an example of VIRTIS spectra averaged over two small areas observed in session 390–13.

[8] A small amount of scattered sunlight is visible in the spectra at short wavelengths (Figure 1). To remove it from the nightside spectra, we used the intensity at $1.061\ \mu\text{m}$ (Spectel 4) and $1.232\ \mu\text{m}$ (Spectel 22), two wavelengths at which no nightside emission is expected from synthetic models. We assumed a linear spectral variation for this scattered component between these two wavelengths. The so-calculated scattered light also reproduces the residual intensity at $1.356\ \mu\text{m}$ (Spectel 35), another wavelength at which models predict no nightside emission.

[9] We found that the wavelength scale of the observations was slightly shifted from that given in the spectral cubes after the latest calibration of the VIRTIS VEX archive (v2.1, 18 March 2008). In the sequences selected, this shift

Table 1. VIRTIS Nightside Sequences^a

Session ^b	Date	Science Case	Exposure Time (sec)	Maximum and Minimum Latitudes	Easternmost and Westernmost Longitudes	Comment
093–01	22 Jul 2006	3	3.3	7; –61	178; 247	includes Imdr Regio
157–03	25 Sep 2006	2	3.3	–8; –44	331; 6	includes Alpha Regio
390–09	16 May 2007	2	8	9; –68	323; 29	
390–13	16 May 2007	2	8	17; –56	331; 23	includes Alpha Regio
392–05	17 May 2007	2	8	–34; –85	328; 119	
392–06	17 May 2007	2	8	–29; –82	337; 114	
571–08	12 Nov 2007	2	3	5; –61	199; 269	includes Imdr Regio
571–11	12 Nov 2007	2	3	–8; –70	245; 311	includes Themis Regio
577–06	18 Nov 2007	2	8	10; –56	279; 327	
577–08	18 Nov 2007	2	8	14; –55	223; 281	
577–10	18 Nov 2007	2	8	15; –50	186; 229	
579–02	20 Nov 2007	2	8	–46; –90	178; 340	
579–06	20 Nov 2007	2	8	9; –57	276; 333	
579–08	20 Nov 2007	2	8	14; –55	228; 287	
579–10	20 Nov 2007	2	8	16; –50	192; 243	
579–12	20 Nov 2007	2	8	23; –31	229; 265	

^aVisible and Infrared Thermal Imaging Spectrometer.

^bSessions in bold are those used to derive the CO₂ continuum opacity (section 4.2).

varies between approximately 0.75 and 0.95 time the spectral size (9.5 nm). It varies reproducibly along the 256-pixel slit by 0.1 pixel, reaching a maximum around Pixel 100 (see section 5 and Figure 7). We considered this spectral shift as a free parameter in the fitting procedure used to derive the water vapor abundance.

3. Radiative Transfer Model

[10] Synthetic spectra were calculated using a line-by-line radiative transfer model with scattering originally developed to analyze high-resolution spectra of Venus’ night side [Bézard *et al.*, 1990; de Bergh *et al.*, 1995]. We improved over these earlier works by employing the Discrete Ordinates Radiative Transfer Program for a MultiLayered Plane-Parallel Medium (DISORT) algorithm [Stamnes *et al.*, 1988] with eight streams to solve the equation of transfer in place of a Delta-Eddington adding algorithm. A Henyey-Greenstein phase function was used for particle scattering. The temperature profile, assumed to be horizontally uniform, is based on entry probe data at low latitudes, as compiled by Seiff [1983, Table A1]. We did not update these data, the VIRA-2 profile [Moroz and Zasova, 1997] being the same as the VIRA one in the lower atmosphere. The CO₂ mole fraction is 0.965 and the H₂O profile is assumed constant with height below the clouds. Rayleigh scattering by CO₂ is included. Surface emissivity was arbitrarily set to 0.95. We used the simplified cloud model described by Crisp [1986] that extends from 30 to 80 km. Extinction efficiencies, single scattering albedos and asymmetry parameters were generated layer by layer by calculating Mie scattering by four modes of 75% H₂SO₄ particles.

[11] For CO₂ line opacity, we used the high-T database presented by Pollack *et al.* [1993], while the H₂O line parameters come from Geisa 97 [Jacquinot-Husson *et al.*, 1999]. The CO₂ self-broadened half width was taken as 0.1 cm^{–1} atm^{–1} and varying as T^{–0.75}. For CO₂-broadened H₂O line half widths, we used a routine provided by R.H. Tipping and R. Freedman (private communication, 2000). We used a Voigt profile for the H₂O lineshape with a cutoff at 120 cm^{–1} from line center. For CO₂ lines, we

assumed the following sublorentzian lineshape (with a cutoff at 180 cm^{–1} from line center):

$$\begin{aligned} \Delta\sigma < 3 : \chi &= 1 \\ 3 < \Delta\sigma < 60 : \chi &= 1.051 \exp(-\Delta\sigma/60) \\ 60 < \Delta\sigma : \chi &= 0.6671 \exp(-\Delta\sigma/110), \end{aligned}$$

where $\Delta\sigma$ is the distance from line center expressed in cm^{–1} and χ is the factor by which we multiply the Voigt lineshape. This χ factor was found to best reproduce the low-frequency side of the 1.18- μ m window, dominated by CO₂ absorption, as observed in high-resolution ground-based spectra [de Bergh *et al.*, 1995]. Various analyses of the Venus nightside windows have shown that an additional continuum opacity, likely due to collision-induced CO₂ bands and/or extreme far wings of strong allowed CO₂ bands, is a major contributor to the gas opacity. Its strength may be relatively well determined in the 2.3- and 1.74- μ m windows by fitting the amplitude of allowed CO₂ lines in high-resolution spectra [e.g., Bézard *et al.*, 1990; Pollack *et al.*, 1993; de Bergh *et al.*, 1995]. This is not the case for the 1.18- and 1.1- μ m windows where no marked CO₂ feature is present. Fortunately, it is possible to take advantage of the transparency of these two windows and thus of their sensitivity to the surface elevation to determine this “continuum” opacity, as shown in section 4. We parameterize it with a constant binary absorption coefficient, expressed in cm^{–1} amagat^{–2}.

[12] For each spectral selection we analyzed, we used the mean outgoing intensity from our model (i.e., the upward flux divided by π) and rescaled it by a factor f to reproduce the observed 1.18- μ m intensity. This factor accounts for the variation in emission angle and cloud opacity from one selection to another. This simplified approach is valid because these two parameters are spectrally neutral and uniformly modulate the outgoing intensity. To check this, we calculated the radiance ratios of spectra at various emission angles up to 80° to that at zero emission angle. Figure 2 shows that these ratios are quasi-constant across the 1.18- μ m window, with a variation less than 1%. The water vapor signature is thus fully preserved in changes of

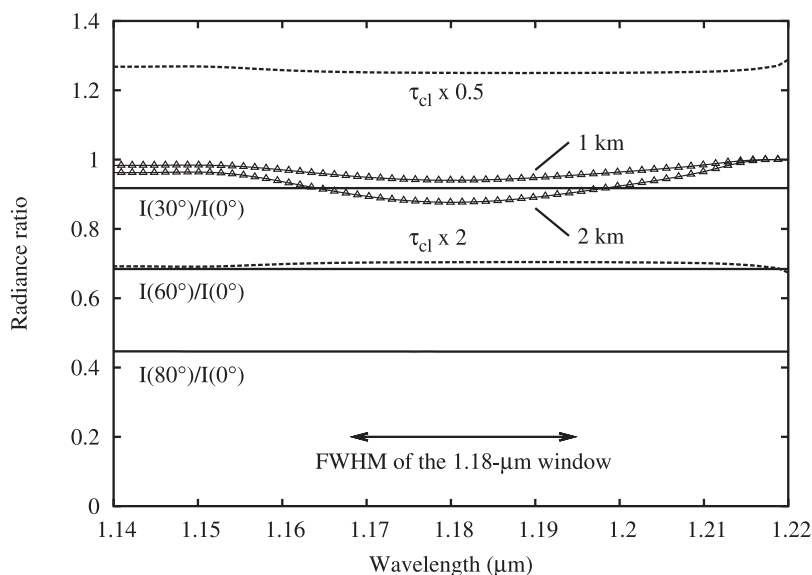


Figure 2. Ratios of synthetic spectra calculated at 17-nm resolution for different emission angles (solid lines), twice and half the optical depth of the lower cloud layer (dashed lines), and for surface elevation of 1 and 2 km (lines with triangles). In all cases, the reference spectrum corresponds to the nominal cloud model described in the text, a zero surface elevation, and a zero emission angle.

the emission angle and the mean intensity throughout the window is proportional to the intensity at any emission angle. This occurs because the clouds are optically thick and located well above the line-forming region. In Figure 2, we also show the radiance ratios of models in which the cloud optical depth in the middle and lower cloud layers (below 57 km) is equal to half and twice that in the nominal model. A negligible variation of these ratios across the window is found (less than 1%). Cloud scattering therefore acts a gray attenuator (or a scaling factor) and does not modify the spectral shape of the window because it takes place well above the line-forming region at $1.18 \mu\text{m}$ with negligible thermal emission by the particles themselves. This also means that our water vapor retrievals are not sensitive to uncertainties in our cloud model.

4. Determination of the Water Vapor Abundance

4.1. Spectral Resolution of VIRTIS-M Observations

[13] A precise knowledge of the spectral resolution of the VIRTIS spectra is important for an accurate determination of the H_2O abundance, all the more as the wavelength calibration of the data is not known to better than about half a spectel. Water vapor absorption affects the width of the $1.18\text{-}\mu\text{m}$ window so that an error in the spectral resolution can be offset to first order by a change in the H_2O abundance and a slight variation in the pixel registration. The spectral profile of the VIRTIS-M infrared channel, around the center of the slit, has been measured before launch. The profile could be fit with a Gaussian having a full width at half maximum (FWHM) of $11.0 \pm 1.2 \text{ nm}$. However, synthetic spectra convolved with this profile do not match the VIRTIS Venus nightside spectra, as evidenced at $1.74 \mu\text{m}$, the narrowest window. To determine the actual resolution of the observations, we used this window and compared VIRTIS spectra to high-resolution ground-based

spectra recorded at the Canada-France-Hawaii telescope (CFHT) by one of us (BB), Catherine de Bergh, Dave Crisp and Jean-Pierre Maillard [Taylor et al., 1997, Figure 4]. We convolved the latter spectrum with Gaussian functions having different FWHMs and determined the best value through a least squares fit. Figure 3 shows the result for the Alpha Regio spectrum of Figure 1: The CFHT spectrum convolved at 11 nm resolution is too narrow compared to the VIRTIS spectrum and does not produce enough emission in the wings of the window whereas a FWHM of 17 nm yields a very good fit. We found that, among the VIRTIS sessions marked in bold in Table 1, the FWHM of the $1.74\text{-}\mu\text{m}$ window varies between 15 and 19 nm. We used the so-inferred resolution to analyze the $1.18\text{-}\mu\text{m}$ window. The actual resolution of the VIRTIS-M infrared spectra thus appears to be at least 50% larger than measured in the laboratory owing to different temperatures of the spectrometer (135 K for the laboratory measurement versus around 150–160 K in orbit).

4.2. Determination of the CO_2 Continuum Absorption

[14] As discussed in section 3, the presence of an unknown continuum opacity in the windows, likely due to CO_2 collision-induced bands or extreme far wings of strong allowed bands, adds some uncertainty in the composition retrievals. To constrain this quantity, we analyzed VIRTIS $1.18\text{-}\mu\text{m}$ spectra taken over regions of different elevations during the same session. The contrast between high and low elevation spectra, due to differences in surface temperatures, is sensitive to the gas opacity, e.g., a larger continuum absorption increases the atmospheric opacity, attenuates more strongly the surface emission from lower elevations, and thus diminishes the contrast. In five different sessions, we selected spectra over areas at relatively high elevation (Alpha Regio, Themis Regio or Imdr Regio) and at low elevation. We used the altimetry derived from Magellan and

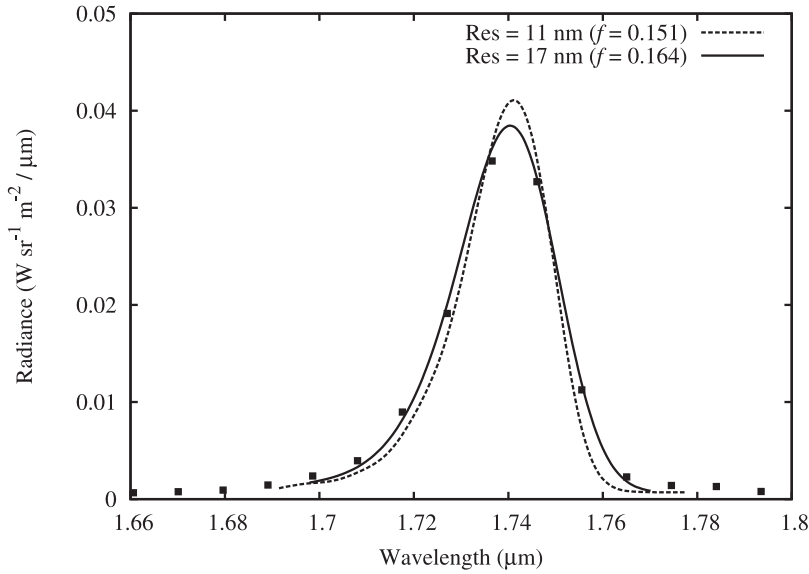


Figure 3. The 1.74- μm VIRTIS spectrum of Alpha Regio in Figure 1 (squares) is compared with Canada-France-Hawaii telescope (CFHT) spectra convolved with a Gaussian function having full width at half maximum (FWHMs) of 11 nm (dashed line) and 17 nm (solid line). In each case, a multiplying factor f that minimizes the sum of squares of residuals is applied to the CFHT data, a $0.0007 \text{ W sr}^{-1} \text{ m}^{-2} \mu\text{m}^{-1}$ is added to account for residual scattered sunlight in the instrument, and a wavelength shift $\lambda_{\text{shift}} = 6.8 \text{ nm}$ is applied to the VIRTIS spectrum.

smoothed it with a boxcar average of width 80–100 km to account for blurring by the overlying cloud layers [e.g., Moroz, 2002]. The spectral samples, listed in Table 2, comprise 12 to 285 spectra.

[15] Besides elevation, the intensity of the emission at 1.18 micron is also dependent on the emission angle and the cloud opacity. We then corrected the spectra to zero emission angle using the limb-darkening model derived by Carlson et al. (manuscript in preparation, 2008) and we used the peak intensity in the windows at 1.27, 1.31 and 1.74 microns, not probing down to the surface, as an indicator of the cloudiness. The 1.31- μm window (Spectel 30) is in principle best suited for this purpose [Meadows and Crisp, 1996] but it is weak and has a relatively low

signal-to-noise ratio. The 1.28- μm intensity at Spectel 27 is stronger but slightly contaminated by the 1.27- μm O_2 airglow peaking at Spectel 26. The 1.74- μm window (Spectel 76) has a very good signal-to-noise ratio but, being at much longer wavelengths, it is not a perfect indicator of the cloud opacity at 1.18 μm : spectra with similar 1.74- μm radiances can differ at 1.18 μm owing to different particle size characteristics as was investigated from Galileo/NIMS data in the case of the 2.3- and 1.74- μm windows by Carlson et al. [1993]. To select low elevation regions having similar cloudiness as the high elevation regions, we used a combination of these three windows and empirically imposed intensity variations less than 4% at 1.28 μm , 6% at 1.31 μm and 15% at 1.74 μm . In each session, we

Table 2. VIRTIS Nightside Spectra Used to Determine the CO_2 Continuum Opacity and H_2O Mole Fraction

Session	Pixel Range ^a	Mean Latitude and Longitude	Mean Local Time	Mean Altitude (km)	Mean Emission Angle (deg)	H_2O Mole Fraction ^b (ppm)
093-01	120-122; 70-73	-46.4; 214.8	23.10	2.58	36	42 \pm 3
093-01	85-92; 73-79	-43.4; 220.7	22.68	-0.03	38	43 \pm 3
093-01	134-143; 95-103	-41.4; 208.7	23.48	1.35	43	41 \pm 3
093-01	144-158; 61-66	-48.8; 208.2	23.51	-0.14	35	39 \pm 3
157-03	64-71; 214-220	-26.0; 359.2	2.76	1.68	28	39 \pm 4
157-03	88-96; 177-183	-26.5; 355.0	3.04	-0.37	26	41 \pm 4
157-03	19-27; 88-96	-36.9; 351.9	3.24	-1.11	15	47 \pm 5
390-13	112-130; 149-163	-26.6; 359.9	21.38	1.30	45	43 \pm 3
390-13	141-159; 126-140	-25.9; 354.8	21.04	-0.47	45	42 \pm 3
390-13	69-80; 147-163	-31.7; 4.2	21.66	0.13	41	45 \pm 3
571-08	218-220; 78-81	-46.2; 214.6	22.61	2.68	32	49 \pm 4
571-08	248-254; 58-65	-46.8; 206.8	22.09	0.02	33	51 \pm 4
571-11	93-97; 137-145	-40.8; 277.4	21.22	2.06	37	49 \pm 4
571-11	88-98; 33-43	-51.5; 291.1	20.30	-0.07	32	54 \pm 5
571-11	131-139; 138-159	-43.5; 270.2	21.69	-0.17	32	48 \pm 5

^aAlong the slit; across the slit.

^bAssuming a CO_2 continuum absorption of $1.1 \times 10^{-9} \text{ cm}^{-1} \text{ amagat}^{-2}$.

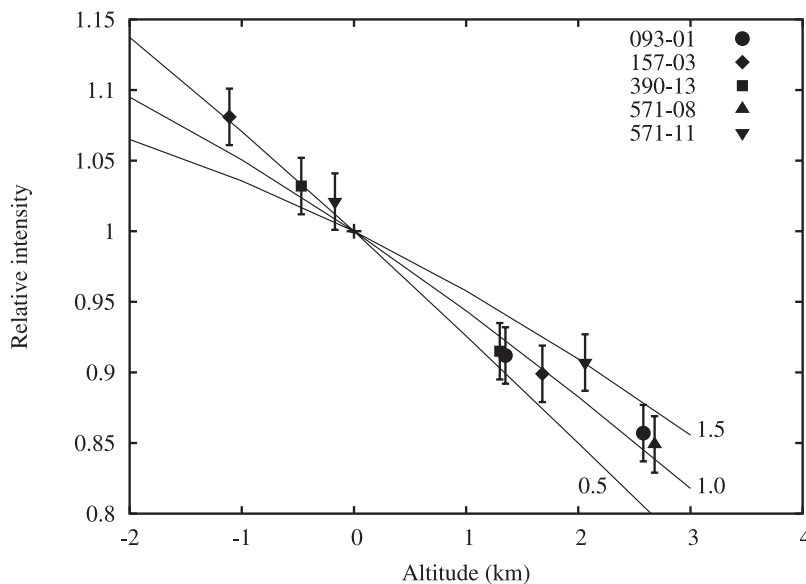


Figure 4. Relative variations of the intensity at $1.185 \mu\text{m}$ as a function of surface elevation for the Visible and Infrared Thermal Imaging Spectrometer (VIRTIS) spectral selections in Table 2 (symbols). Model variations for different continuum opacity ($0.5, 1.0,$ and $1.5 \times 10^{-9} \text{ cm}^{-1} \text{ amagat}^{-2}$) are shown for comparison.

chose a region around 0 km altitude and, if possible, one at a lower elevation. Figure 1 shows two averaged spectra from session 390–13, one at 1.30 km and the other one at -0.47 km. One clearly sees that the intensities at 1.1 and $1.18 \mu\text{m}$ are larger for the low elevation spectrum whereas the intensities in the 1.27, 1.31 and $1.74\text{-}\mu\text{m}$ windows are similar in the two spectra, which indicates similar cloudiness.

[16] Figure 4 shows the relative intensity observed at Spectel 17 ($\sim 1.185 \mu\text{m}$) for the highest and lowest elevations of each session with respect to that at 0 km altitude in the same session. We estimate that each datum point bears an uncertainty of ± 0.02 owing to the cloud opacity. A least square fit to these data indicates a variation of the intensity of $-5.7 \pm 0.4\%$ per km. Comparison with model calculations indicates that a constant absorption coefficient of $1 \pm 0.4 \times 10^{-9} \text{ cm}^{-1} \text{ amagat}^{-2}$ best reproduces the observed variation. The corresponding optical depth at 0 km is 0.92, larger than that due to H_2O lines (0.36 for a mole fraction of 40 ppm) and CO_2 lines (0.68) at $1.182 \mu\text{m}$ and 17-nm resolution, which shows that this continuum opacity is an important contributor to the gaseous absorption in this window. The Rayleigh scattering optical depth is 0.65. We checked that changing the surface emissivity (from 0.95 to 0.80) does not significantly affect the derived continuum absorption coefficient.

4.3. Determination of the H_2O Mole Fraction

[17] To determine the water vapor abundance, we fitted the spectra in Table 2 with synthetic models calculated with the above determined continuum opacity and various H_2O mole fractions. For each value of H_2O , we determined the values of the spectral shift λ_{shift} and scaling factor f (related to cloud opacity and emission angle) that provide the best fit of the $1.18\text{-}\mu\text{m}$ VIRTIS spectrum and calculate the residuals of the fit. We then retained the value of the H_2O mole fraction that minimizes the sum of squares of these resid-

uals. In Figure 5, the Alpha Regio spectrum (Figure 1) is compared to synthetic spectra calculated with 30, 40 and 55 ppm of H_2O , which shows the strong effect of water vapor absorption on the spectra. Figure 6 shows that the two spectra of Figure 1 that have different surface elevations are well fitted with a continuum absorption coefficient of $1 \times 10^{-9} \text{ cm}^{-1} \text{ amagat}^{-2}$ and a water mole fraction of 40 ppm (the same spectral shift and scaling factor are applied to both spectra).

[18] The H_2O mole fraction that best reproduces the spectral selections, assuming a continuum absorption coefficient of $1.1 \times 10^{-9} \text{ cm}^{-1} \text{ amagat}^{-2}$, is indicated in the last column of Table 2 with the 1 SD error bar derived from the residuals of the fit. The weighted mean value is 45 ppm (44 ppm if a continuum absorption coefficient of $1 \times 10^{-9} \text{ cm}^{-1} \text{ amagat}^{-2}$ is used) and the standard deviation of the sample is 5 ppm. The $\pm 40\%$ uncertainty on the CO_2 continuum absorption adds a ± 3 ppm uncertainty on the H_2O mole fraction and the estimated $\pm 10\%$ uncertainty on the VIRTIS-M spectral resolution at $1.18 \mu\text{m}$ adds another ± 7 ppm. Combining quadratically all these uncertainties, we conclude that the H_2O mole fraction in the lowest scale height of the atmosphere is 44 ± 9 ppm. Note that this uncertainty does not take into account any possible inaccuracies or incompleteness in the H_2O spectral database used here (Geisa 97).

5. Search for Horizontal Variations

[19] We searched for possible variations of the H_2O abundance in the sequences listed in Table 1. Besides the H_2O abundance, the intensity of the $1.18\text{-}\mu\text{m}$ window emission is sensitive to the cloud optical depth, emission angle and surface elevation (Figure 2), all of which vary spatially. It is thus necessary to correct the images for the variations in these parameters or to work on quantities that

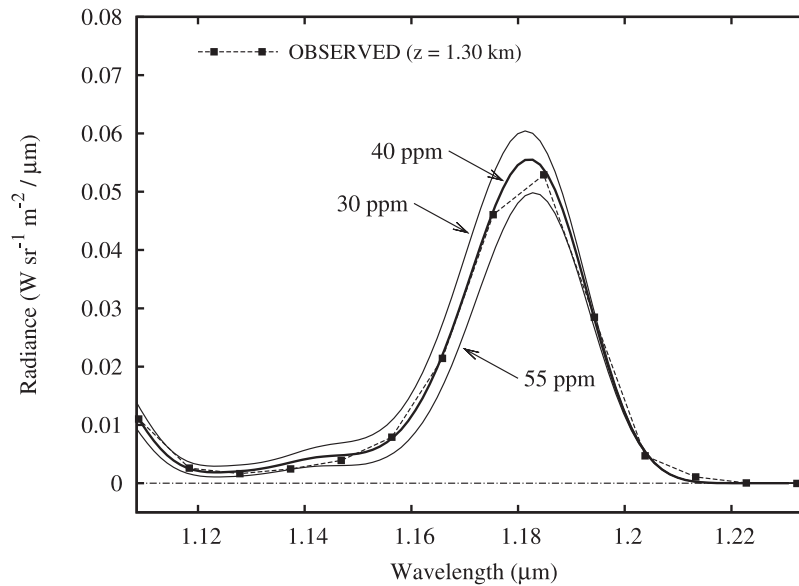


Figure 5. The Alpha Regio spectrum of Figure 1 is compared to synthetic spectra with H₂O mole fractions of 30, 40, and 55 ppm. The spectral shift $\lambda_{\text{shift}} = 7.9$ nm and scale factor $f = 0.78$ are those that yield the best fit of the data with the 40-ppm calculation.

are least sensitive to them. The effect of the first two parameters is spectrally neutral across the window (Figure 2) and can therefore be eliminated by ratioing the intensity at two wavelengths. A complication arises from the fact that the spectral registration is not constant along the slit as mentioned above and that the spectral resolution may also slightly vary. The first step is thus to determine the spectral shift for each pixel of the images. This was done by determining the peak of the 1.18- μm window from a parabolic fit of the intensity at spectels 16, 17 and 18 and assigning it to 1.182 μm , as determined from synthetic

calculations (Figure 6). The result is shown for a particular sequence (579–08) in Figure 7. In all sequences, the spectral shift increases by ~ 1 nm (~ 0.1 spectel) along the slit from Pixel 6 up to Pixels ~ 80 –100 and slightly decreases beyond. The variation of the spectral shift in the scan direction, i.e., during the acquisition, is negligible for this sequence (Figure 7) and all those investigated here.

[20] We first considered the ratio R_1 of the intensity at 1.169 μm to that at the peak of the window (1.182 μm) to map water vapor variations. The first wavelength lies in the wing of the window that is dominated by H₂O absorption.

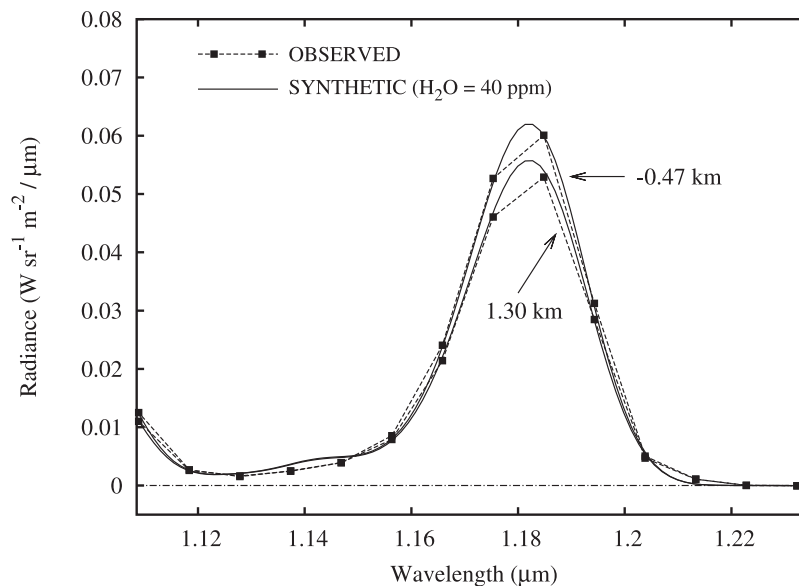


Figure 6. The two spectra of Figure 1 (session 390–13) at elevations of 1.30 and -0.47 km are compared with our best fit model that includes a constant absorption coefficient of $1 \times 10^{-9} \text{ cm}^{-1} \text{ amagat}^{-2}$ and a H₂O mole fraction of 40 ppm. The same spectral shift and scale factor as in Figure 5 are used for both spectra.

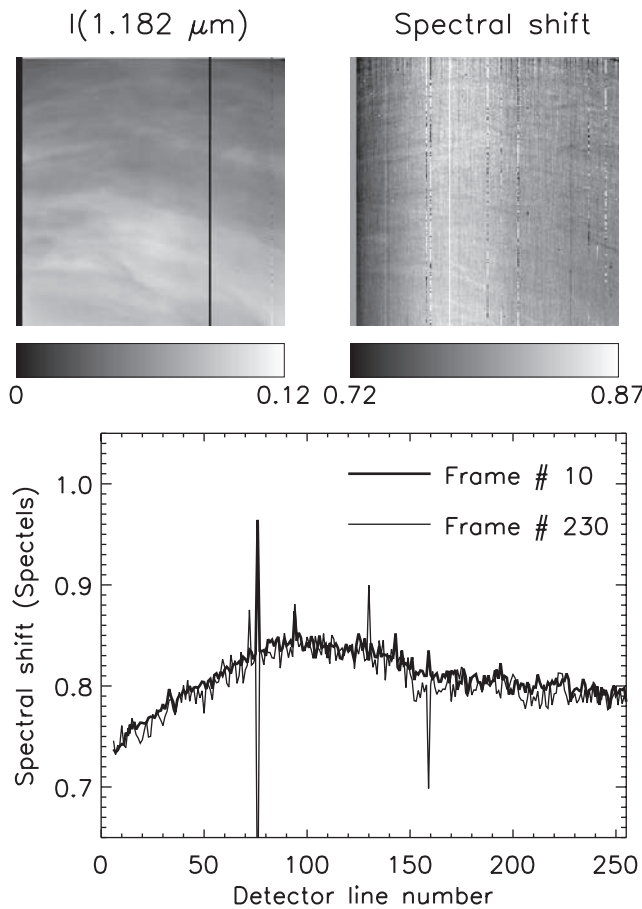


Figure 7. (top) Map of the 1.182- μm intensity ($\text{W sr}^{-1} \text{m}^{-2} \mu\text{m}^{-1}$) in sequence 579–08 and of the spectral shift, expressed as a fraction of a spectel, with respect to the VIRTIS/Venus Express archive calibration (v2.1). (bottom) Plots of the shift as a function of detector line number along the slit for two different frames (i.e., image lines).

The intensity at 1.182 μm is derived from the above mentioned parabolic fit and that at 1.169 μm is interpolated linearly between the two adjacent spectels. Synthetic calcu-

lations show that a 10% variation of the H_2O mixing ratio yields a 3.5% variation of this ratio. Because this ratio is potentially very sensitive to remaining uncertainties in the spectral registration, we considered a second parameter (W), which is the FWHM of the window. Calculations indicate that a 10% variation of the H_2O mixing ratio yields a 2.3% variation of this quantity. The maps of these two quantities are shown in Figure 8 for sequence 579–08. Clearly, the effect of cloud opacity and emission angle variations is very well removed as attested by comparing to the 1.182- μm image. However, features remain that are not due to water vapor variations. First, there is a slight increase of the two parameters R_1 and W with increasing pixel number along the slit (from left to right in Figure 8) for all image lines. This probably reflects a slight increase of the spectral width of the instrumental function from the beginning (small detector line numbers) to the end (large detector line numbers) of the 256-pixel slit. Second, topographic features are clearly seen in the R_1 and W images and actually a very good correlation is observed with the altimetry map also shown in Figure 8. This occurs because altitude variations affect more the peak of the window, where the gas opacity is at minimum, than its wings. A higher altitude region is therefore characterized by a larger value of R_1 and a larger FWHM as the 1.182- μm intensity is more strongly reduced than those at half maximum in the wings. Consequently, we defined a third parameter R_2 to minimize the influence of the topography and of the spectral resolution, that is the ratio of the intensity in the CO_2 wing at 1.1945 μm to that in the H_2O -dominated wing at 1.169 μm . These two wavelengths exhibit similar intensities and probe similar atmospheric levels so that their intensity ratio is not too sensitive to the surface altitude. Synthetic calculations indicate that this ratio shows little sensitivity to small variations of the spectral resolution and that a 10% variation in the H_2O mixing ratio causes a 5% variation of this intensity ratio R_2 .

[21] The map of the R_2 ratio, shown in Figure 8, is bland except for the hot pixels, which confirms that all the effects above mentioned have been removed with a very good accuracy. Figure 9 shows cuts through this image with peak-to-peak variations of about 3%, attributable to noise and a

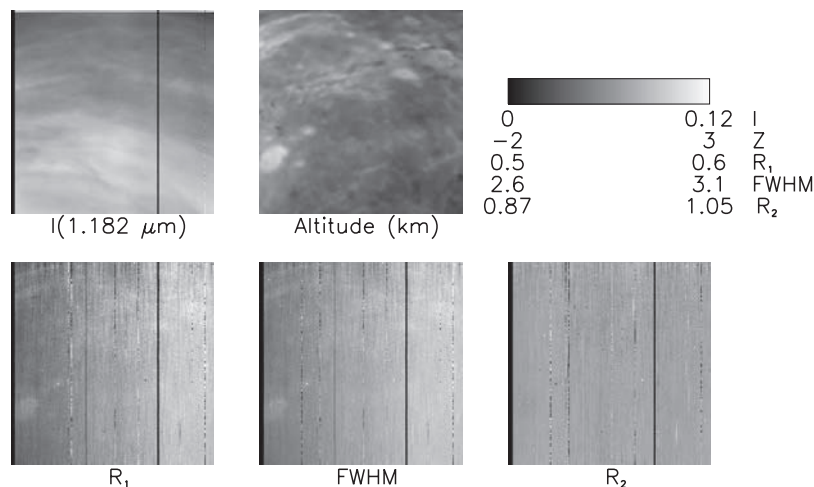


Figure 8. Maps of the 1.182- μm intensity I ($\text{W sr}^{-1} \text{m}^{-2} \mu\text{m}^{-1}$), smoothed surface elevation Z (km), ratio of the intensity at 1.169 and 1.182 μm (R_1), FWHM of the window (spectels), and ratio of the intensity at 1.1945 and 1.169 μm (R_2) for sequence 579–08.

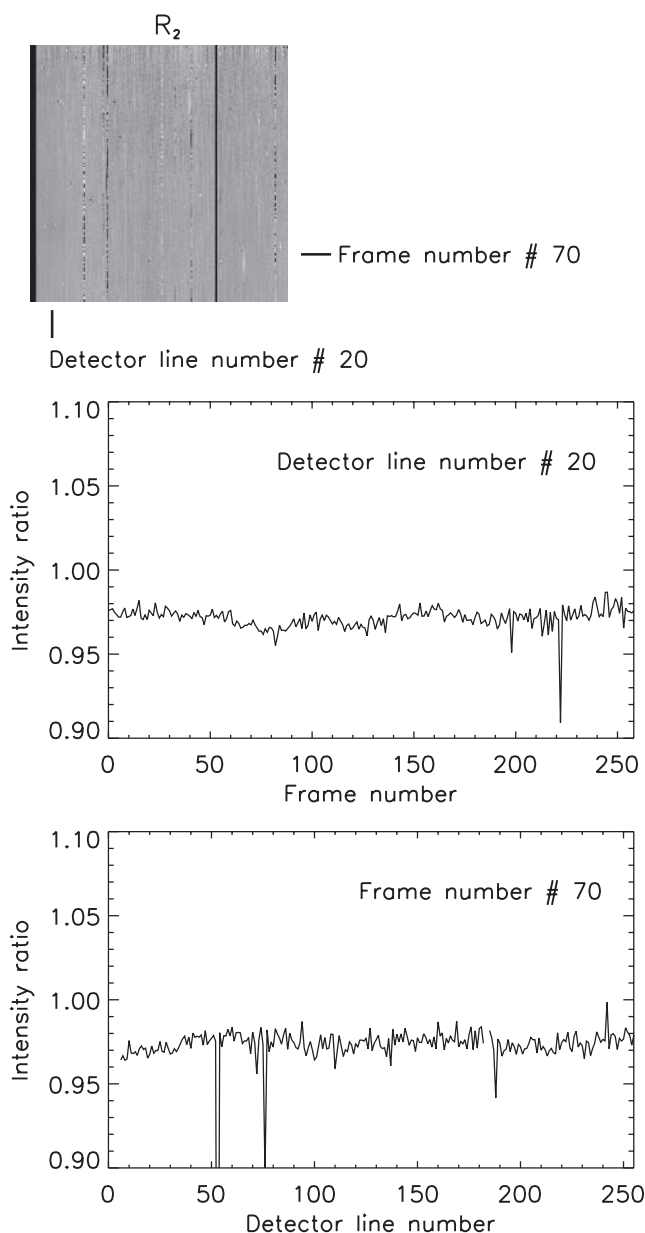


Figure 9. Image of the 1.1945- to 1.169- μm intensity ratio (R_2) shown in Figure 8, and cuts of this image at line (frame) 70 and at column (detector line) 20.

residual altitude signature at the 1% level. We have calculated the median of R_2 in latitude boxes 5° wide (Figure 10) and found no variations beyond $\pm 0.3\%$ from the mean from 60°S to 15°N for this sequence 579–08. The same analysis was performed for all sequences in Table 1 (examples shown in Figure 10). Data southward of 80°S cannot be used owing to a large amount of scattered light from the dayside. Note that for some sequences, having a lower spectral shift than in most cases, we used other wavelengths to calculate the R_2 ratio (namely 1.1905 and 1.1685 μm), which allows us to better correct the above mentioned effects. We do not see any significant variations of the R_2 intensity ratio with latitude in any sequence and we place an upper limit of $\pm 0.5\%$ for the range 60°S – 25°N . The data poleward of 60°S are somewhat affected by scattered light

from the day side and we set an envelope of $\pm 1\%$ for any possible latitudinal variation in the whole range 80°S – 25°N . These upper limits translate into $\pm 1\%$ (± 0.5 ppm) for the H_2O mixing ratio in the range 60°S – 25°N and $\pm 2\%$ (± 1 ppm) for the broader range 80°S – 25°N .

6. Discussion

[22] The absorption coefficient we inferred for the additional continuum opacity in the 1.18- μm window ($1 \pm 0.4 \times 10^{-9} \text{ cm}^{-1} \text{ amagat}^{-2}$) agrees with that derived independently by *Carlson et al.* (manuscript in preparation, 2008) from VIRTIS and Galileo/NIMS data. Both analyses assume a temperature lapse rate from the VIRA model [*Seiff, 1983*] in all investigated regions. If it is shallower (and thus more stable) than in the VIRA model, as argued by *Meadows and Crisp [1996]*, a smaller continuum opacity would be needed. Also, our analysis relies on the assumption of constant surface emissivity at 1.18 μm over the regions we investigated. If, for example, the surface emissivity instead decreases with elevation in the near-infrared as it generally does in Magellan radar images, a larger continuum opacity would be needed to reproduce the observed intensity variation. To our knowledge, we provide here the first determination of this continuum opacity, which is very difficult to measure in the laboratory as it requires very large optical path lengths and high temperatures.

[23] Having constrained this important source of opacity, we could determine the H_2O mole fraction with a relatively good accuracy. The result, 44 ± 9 ppm, pertains to the 0–15 km range. It agrees with most previous determinations as reviewed by *Bézard and de Bergh [2007]*, in particular with that of *Meadows and Crisp [1996]* (45 ± 10 ppm). We do not have any vertically resolved information given the small range of surface elevation in the data sets we analyzed (~ 3 km) and therefore we cannot discriminate between the somewhat different conclusions of *Meadows and Crisp [1996]* and *Ignatiev et al. [1997]*. From ground-based observations of the 1.0, 1.1 and 1.18- μm windows and using the topography for altitude resolution, *Meadows and Crisp* concluded that the H_2O mole fraction was constant (within $\pm 10\%$) in the lowest scale height (0–15 km) at a value of 45 ± 10 ppm. In contrast, from a reanalysis of the Venera optical spectra, *Ignatiev et al. [1997]* argued that the H_2O mole fraction probably increases from about 20 ppm at 10–20 km to 50–70 ppm below 5 km. Both distributions yield column-averaged mixing ratios (45 and 37 ppm respectively) that agree with our result within error bars.

[24] It is important to note that our determination was obtained using the Geisa 97 database for the H_2O absorption. Given the large optical paths and high temperatures involved, it is possible that weak high-energy lines, not included in Geisa (or Hitran), provide a significant contribution in the H_2O wing of the 1.18- μm window. If this was the case, the mole fraction needed to reproduce the 1.18- μm observations would probably be lower than the 44 ppm we derived.

[25] The 2.3- μm nightside window gives the opportunity to measure the water abundance at higher altitudes, in the range ~ 30 –45 km. A recent analysis of VIRTIS-H spectra indicates a mixing ratio of 31 ± 2 ppm [*Marcq et al., 2008*], where the error bars derive from the residuals of the fits and

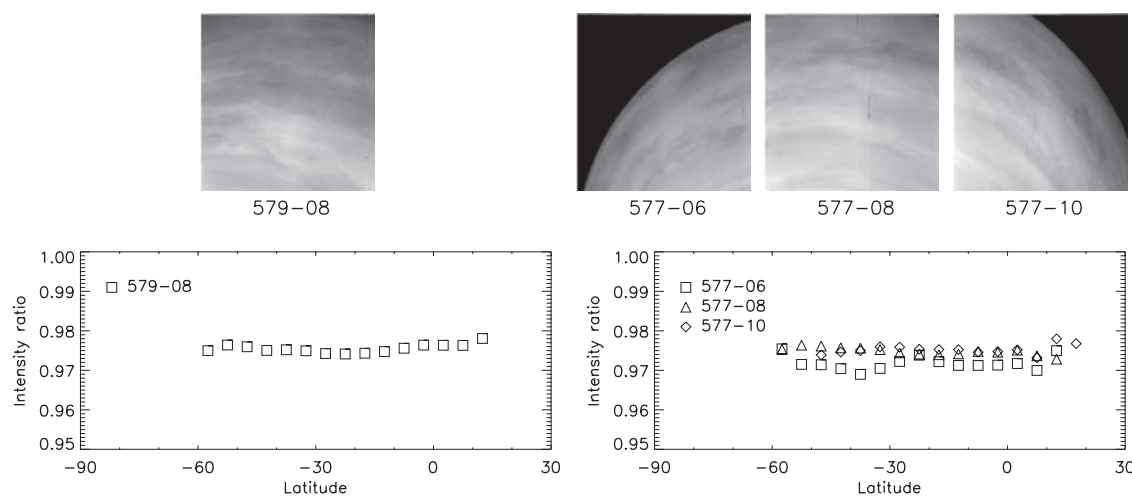


Figure 10. Variations of the intensity ratio R_2 with latitude in sequences 579–08, 577–06, 577–08, and 577–10. Images of these sequences at $1.182 \mu\text{m}$ are also shown.

do not account for systematic errors such as in the CO_2 continuum absorption. This result is consistent with previous ground-based observations, which indicated 30 ± 10 ppm (see review by *Taylor et al.* [1997]). Emission in the $1.74\text{-}\mu\text{m}$ window is also sensitive to water vapor absorption and originates from 15 to 25 km, a region intermediate between those probed at 2.3 and $1.18 \mu\text{m}$. Ground-based observations of this window again indicate a mole fraction of 30 ± 10 ppm [*Pollack et al.*, 1993; *de Bergh et al.*, 1995]. The 2.3- and $1.74\text{-}\mu\text{m}$ results preclude the large abundance (67 ppm) derived from the Pioneer Venus mass spectrometer measurements [*Donahue and Hodges*, 1992].

[26] Taken at face value, our H_2O mole fraction is about 50% larger than that derived at 2.3 and $1.74 \mu\text{m}$, which suggests an increase of the water abundance in the lowest scale height of the atmosphere. However, given the error bars, we feel that a constant mole fraction around 30–40 ppm from below the clouds down to the surface is still consistent with all analyses of Venus’ nightside emission. A uniform profile agrees with chemical models, which do not predict a significant variation of the H_2O mole fraction between 0 and ~ 38 km [*Krasnopolsky*, 2007]. Below the clouds, the only significant sink for H_2O is formation of H_2SO_4 vapor above 38 km. At 40 km, the H_2O mole fraction is depleted by about 2 ppm and at 45 km by about 7 ppm [*Krasnopolsky*, 2007]. The $2.3\text{-}\mu\text{m}$ window has some weak sensitivity to the 40–45 km region and high spectral resolution observations might be able to measure this decrease with height. If real, the strong increase of the water mole fraction below 5 km suggested by *Ignatiev et al.* [1997] would imply a source at or near the surface and a sink above 5 km that are not predicted by existing chemical models and remain to be identified.

[27] We have obtained very stringent upper limits for any variation of the H_2O mole fraction at 0–15 km with latitude in several VIRTIS-M sequences: ± 0.5 ppm in the range 60°S – 25°N and ± 1 ppm if we extend the range to 80°S – 25°N . *Drossart et al.* [1993] previously searched for H_2O variations using the same $1.18\text{-}\mu\text{m}$ window in the Galileo/NIMS data. This study was limited to three narrow north to south strips covering small areas between 40°S and 50°N .

No variation exceeding $\pm 20\%$ (± 6 ppm) was found in this latitude range ($\pm 10\%$ for the smaller range 30°S – 30°N). *Marcq et al.* [2006] searched for horizontal variations of H_2O in their NASA/IRTF observations of the $2.3\text{-}\mu\text{m}$ nightside window, probing the 30–45 km region. They did not see any beyond $\pm 15\%$ (± 4 ppm) in the latitude range 40°S – 40°N . In contrast, CO shows a 30–40% increase from the equator to 60°S at ~ 36 km and an anticorrelated decrease of OCS at ~ 33 km [*Marcq et al.*, 2006, 2008; *Tsang et al.*, 2008]. These variations are interpreted as the signature of the large-scale circulation, with upwelling at the equator and downwelling at high latitudes, in the presence of vertical gradients of CO and OCS due to chemical sources and sinks. The fact that we do not see any variations of the H_2O abundance in the first scale height of the atmosphere is fully consistent with the constancy of the vertical profile with height below 40 km and the absence of significant sources and sinks. A contrario, our result probably precludes the factor of 2–3 increase of the H_2O mole fraction from 10 to 0 km advocated by *Ignatiev et al.* [1997]: General Circulation Model (GCM) calculations by Lebonnois et al. (manuscript in preparation, 2008) suggest an alternance of upward and downward motions from equator to pole in the lowest 20 km, which would probably induce some measurable latitude variation of the H_2O abundance we determined, with larger (smaller) abundances in upwelling (downwelling) regions.

7. Conclusions

[28] Observations of the night side of Venus by the Venus Express/VIRTIS-M instrument in the $1.18\text{-}\mu\text{m}$ atmospheric window have been used to measure and map the distribution of H_2O near the surface of Venus. We have first determined the continuum opacity present in this window from the variation of the peak intensity with surface elevation. This opacity likely results from CO_2 collision-induced bands and far wings of strong CO_2 bands outside the window (beyond 180 cm^{-1} , which is the cutoff we used here), as is the case at $2.3 \mu\text{m}$ [*Tonkov et al.*, 1996]. The absorption coefficient we inferred is $1 \pm 0.4 \times 10^{-9} \text{ cm}^{-1} \text{ amagat}^{-2}$. At the

VIRTIS-M resolution (17 nm), the corresponding optical depth is similar to that due to molecular bands of CO₂ and H₂O. Up to now, CO₂ continuum opacity has been measured only in the 2.3- μ m window and at room temperature [Tonkov et al., 1996]. Laboratory measurements in the 1.18- and 1.1- μ m windows at temperatures relevant to Venus' deep atmosphere would be extremely useful but are very difficult owing to the huge CO₂ path lengths and high temperatures (600–730 K) required.

[29] Analyzing spectral selections in various areas of Venus' southern hemisphere, we derived from radiative transfer calculations a water vapor mole fraction of 44 ± 9 ppm, which pertains to the altitude range 0 to 15 km. The quoted error bars do not include possible errors or incompleteness of the H₂O spectroscopic data used here (Geisa 97). It is highly desirable to assess whether the Geisa or Hitran databases are sufficient to model the H₂O absorption in the 1.18- μ m window. If weak hot lines, not included in these databases, contribute significantly to the opacity, the H₂O mole fraction needed to reproduce the VIRTIS data would probably be lower than inferred here. Besides this caveat, the main source of uncertainty lies in the spectral resolution of the VIRTIS-M observations that varies from orbit to orbit and was determined for each sequence using the narrow 1.74- μ m window. On the other hand, the VIRTIS data have the advantage of an excellent spatial resolution, which permits to obtain spectra at well-defined surface elevations. The limited range of surface elevations (–0.5 to 2.7 km) covered by the present analysis did not allow us to retrieve a vertical profile for water vapor following Meadows and Crisp's [1996] approach. An extension of the Venus Express mission should provide observations of higher terrains, such as Aphrodite Terra, which could constrain the H₂O profile in the ~0–10 km range. This is important to discriminate between a constant with height profile and a large increase or decrease of the mole fraction below 5 km as suggested by some in situ measurements [Ignatiev et al., 1997; Donahue and Hodges, 1992]. The water mole fraction we derived is somewhat larger but still consistent, within error bars, with that determined at higher altitudes from the 2.3- μ m (30–45 km) and 1.74- μ m (15–25 km) nightside emission, which suggests that the water vapor mole fraction is constant below the clouds between 0 and 40 km, as predicted by chemical models [Krasnopolsky, 2007].

[30] We finally searched for spatial variations of the H₂O abundance in various VIRTIS sequences covering altogether a large latitude range (80°S–25°N). To do so, we used the ratio of the intensity in the two wings of the 1.18- μ m window as a proxy. This search was negative and we derived stringent upper limits for any variation of the H₂O mole fraction with latitude: $\pm 1\%$ for the range 60°S–25°N and $\pm 2\%$ if we consider the broader range 80°S–25°N. These constraints are much stronger than those derived by Drossart et al. [1993] ($\pm 20\%$) from Galileo/NIMS spectra over a more limited spatial coverage. The horizontal uniformity of the H₂O abundance is consistent with an abundance profile constant with altitude and with the expected lack of significant sources and sinks below 40 km. In fact, our results likely preclude any strong vertical gradient of the H₂O concentration in the lowest scale height as vertical motions predicted by GCM calculations would then produce

detectable horizontal variations as is the case for CO and OCS near 35 km [Marcq et al., 2006, 2008; Tsang et al., 2008].

[31] **Acknowledgments.** B.B., E.M., and P.D. acknowledge support from Centre National d'Études Spatiales (CNES). G.P. was supported by Agenzia Spaziale Italiana (ASI). We gratefully thank the VIRTIS technical team for their continuous support.

References

- Bézar, B., and C. de Bergh (2007), Composition of the atmosphere of Venus below the clouds, *J. Geophys. Res.*, *112*, E04S07, doi:10.1029/2006JE002794.
- Bézar, B., C. de Bergh, D. Crisp, and J.-P. Maillard (1990), The deep atmosphere of Venus revealed by high-resolution nightside spectra, *Nature*, *345*, 508–511, doi:10.1038/345508a0.
- Carlson, R. W., L. W. Kamp, K. H. Baines, J. B. Pollack, D. H. Grinspoon, T. Encrenaz, P. Drossart, and F. W. Taylor (1993), Variations in Venus cloud particle properties: A new view of Venus's cloud morphology as observed by the Galileo Near-Infrared Mapping Spectrometer, *Planet. Space Sci.*, *41*, 477–485.
- Crisp, D. (1986), Radiative forcing of the Venus mesosphere: I. Solar fluxes and heating rates, *Icarus*, *67*, 484–514, doi:10.1016/0019-1035(86)90126-0.
- Crisp, D., D. A. Allen, D. H. Grinspoon, and J. B. Pollack (1991), The dark side of Venus: Near-infrared images and spectra from the Anglo-Australian Observatory, *Science*, *253*, 1263–1266, doi:10.1126/science.11538493.
- de Bergh, C., B. Bézar, D. Crisp, J.-P. Maillard, T. Owen, J. Pollack, and D. Grinspoon (1995), Water in the deep atmosphere of Venus from high-resolution spectra of the night side, *Adv. Space Res.*, *15*(4), 79–88, doi:10.1016/0273-1177(94)00067-B.
- Donahue, T. M., and R. R. Hodges Jr. (1992), Past and present water budget of Venus, *J. Geophys. Res.*, *97*, 6083–6091.
- Drossart, P., et al. (1993), Search for spatial variations of the H₂O abundance in the lower atmosphere of Venus from NIMS-Galileo, *Planet. Space Sci.*, *41*, 495–504.
- Ignatiev, N. I., V. I. Moroz, B. E. Moschkin, A. P. Ekonomov, V. I. Gnedykh, A. V. Grigoriev, and I. V. Khatuntsev (1997), Water vapour in the lower atmosphere of Venus: A new analysis of optical spectra measured by entry probes, *Planet. Space Sci.*, *45*, 427–438, doi:10.1016/S0032-0633(96)00143-2.
- Jacquinot-Husson, N., et al. (1999), The 1997 spectroscopic GEISA databank, *J. Quant. Spectrosc. Radiat. Transfer*, *62*, 205–254, doi:10.1016/S0022-4073(98)00111-3.
- Krasnopolsky, V. A. (2007), Chemical kinetic model for the lower atmosphere of Venus, *Icarus*, *191*, 25–37, doi:10.1016/j.icarus.2007.04.028.
- Marcq, E., T. Encrenaz, B. Bézar, and M. Birlan (2006), Remote sensing of Venus' lower atmosphere from ground-based IR spectroscopy: Latitudinal and vertical distribution of minor species, *Planet. Space Sci.*, *54*, 1360–1370, doi:10.1016/j.pss.2006.04.024.
- Marcq, E., B. Bézar, P. Drossart, and G. Piccioni (2008), A latitudinal survey of CO, OCS, H₂O, and SO₂ in the lower atmosphere of Venus: Spectroscopic studies using VIRTIS-H, *J. Geophys. Res.*, *113*, E00B07, doi:10.1029/2008JE003074.
- Meadows, V. S., and D. Crisp (1996), Ground-based near-infrared observations of the Venus nightside: The thermal structure and water abundance near the surface, *J. Geophys. Res.*, *101*, 4595–4622, doi:10.1029/95JE03567.
- Moroz, V. I. (2002), Estimates of visibility of the surface of Venus from descent probes and balloons, *Planet. Space Sci.*, *50*, 287–297, doi:10.1016/S0032-0633(01)00128-3.
- Moroz, V. I., and L. V. Zasova (1997), VIRA-2: A review of inputs for updating the Venus International Reference Atmosphere, *Adv. Space Res.*, *19*, 1191–1201, doi:10.1016/S0273-1177(97)00270-6.
- Piccioni, G., et al. (2007), VIRTIS: The Visible and Infrared Thermal Imaging Spectrometer, *Eur. Space Agency Spec. Publ.*, *ESA SP 1295*, 1–27.
- Pollack, J. B., et al. (1993), Near-infrared light from Venus' nightside: A spectroscopic analysis, *Icarus*, *103*, 1–42, doi:10.1006/icar.1993.1055.
- Seiff, A. (1983), Thermal structure of the atmosphere of Venus, in *Venus*, edited by D. M. Hunten et al., pp. 215–279, Univ. of Ariz. Press, Tucson.
- Stamnes, K., S. C. Tsay, W. Wiscombe, and K. Jayaweera (1988), Numerically stable algorithm for discrete-ordinate-method radiative transfer in multiple scattering and emitting layered media, *Appl. Opt.*, *27*, 2502–2509, doi:10.1364/AO.27.002502.
- Taylor, F. W., D. Crisp, and B. Bézar (1997), Near-infrared sounding of the lower atmosphere of Venus, in *Venus II: Geology, Geophysics, Atmo-*

- sphere, and Solar Wind Environment*, edited by S. W. Bougher et al., pp. 325–351, Univ. of Ariz. Press, Tucson.
- Titov, D. V., et al. (2006), Venus Express science planning, *Planet. Space Sci.*, 54, 1279–1297, doi:10.1016/j.pss.2006.04.017.
- Tonkov, M. V., N. N. Filippov, V. V. Bertsev, J. P. Bouanich, N. Van-Thanh, C. Brodbeck, J. M. Hartmann, C. Boulet, F. Thibault, and R. Le Doucen (1996), Measurements and empirical modeling of pure CO₂ absorption in the 2.3- μm region at room temperature: Far wings, allowed and collision-induced bands, *Appl. Opt.*, 35, 4863–4870, doi:10.1364/AO.35.004863.
- Tsang, C. C. C., et al. (2008), Tropospheric carbon monoxide concentrations and variability on Venus from Venus Express/VIRTIS-M observations, *J. Geophys. Res.*, 113, E00B08, doi:10.1029/2008JE003089.
-
- B. Bézard, P. Drossart, and E. Marcq, LESIA, Observatoire de Paris, 5 place Jules Janssen, F-92190, Meudon, France. (Bruno.Bezard@obspm.fr)
- R. W. Carlson, Jet Propulsion Laboratory, MS 183-601, 4800 Oak Grove Drive, Pasadena, CA 91109, USA.
- G. Piccioni, INAF, IASF, via del Fosso del Cavaliere 100, I-00133 Rome, Italy.
- C. C. C. Tsang, Atmospheric, Oceanic and Planetary Physics, Department of Physics, University of Oxford, Clarendon Laboratory, Parks Road, Oxford, OX1 3PU, UK.